表 1. 橈骨遠位端骨折保存的治療のリハビリテーション

	外固定	物理療法	運動療法
0～2 週	肘上あるいは sugar tong 型のシーネ（三角巾固定）	患肢の挙上，クーリング	肩，手指の ROM 訓練
2～4 週	肘下（手関節のみ）	手指のマッサージ	肘の屈曲・伸展運動 前腕の回内外運動 ゴムボールを用いたグリップ運動
4～6 週	外固定除去 夜間，外出時にスプリント固定	気泡浴，渦流浴 手指のマッサージ	手関節の ROM 訓練 （自動運動中心に） [dart throwers motion]
6～8 週	完全フリー	気泡浴，渦流浴	手関節の他動 ROM 訓練 （全 ROM） 手関節屈筋，伸筋の筋力訓練

骨片が背屈転位（Colles 骨折）し，逆に掌屈位で転倒したさいは掌屈転位（Smith 骨折）する．高齢者では遠位骨片が粉砕し，関節内骨折となることが多い．Colles 型で粉砕の程度が少ない単純な関節外骨折では，徒手整復により良好な整復位が得られた場合はギプス固定による保存的治療が選択される．表 1 に一般的な保存的治療とリハビリテーションの流れを示す．外固定は腫脹の強い受傷後早期は主に sugar tongs 型のシーネ固定とし，腫脹の消退後ギプス固定を手関節中間位で MP 関節は完全にフリーとして施行する．橈骨遠位端骨折は高齢者に多く，手指の拘縮をきたしやすい．前述したように手指の自動・他動運動はなるべく早く指導し，腫脹，浮腫と手指の拘縮の防止に努めることが必要である．自動運動は腫脹の消退には有用であるが，強くグリップさせるような自動運動は骨折部での短縮変形を起す危険性があることにも留意する．DRUJ の不安定性や DRUJ への関節内骨折を認める場合は 2 週間肘上まで固定し，その後肘下に変更して回内外運動を許可する．回内外の ROM 訓練は肘を体幹に固定した状態で行う．一般に背屈転位型では尺骨頭の掌側転位をきたしやすく回内制限を，掌屈転位型では尺骨頭は背側転位し回外制限をきたしやすいことを念頭におく．骨癒合の状況にもよるが，通常はおよそ 6 週間で外固定を除去し，手関節の ROM 訓練を始める．

手術的治療としては経皮鋼線固定，プレート固定，創外固定などがある．創外固定は粉砕の強い例などに用いられ，手関節をまたいで固定するタイプ（bridging type）と最近では手関節をまたがないタイプ（non-bridging type）がある．高齢者で bridging type を使用した場合，過牽引を加えると，伸筋および屈筋腱の緊張が増加し，MP 関節伸展，PIP 関節屈曲拘縮をきたしやすい[4]．一方，non-bridging type では早期の手関節運動が可能となる利点があるが，骨折の粉砕例ではその固定力にはなお問題があると思われる．

2 舟状骨骨折

舟状骨骨折は若年者から壮年にかけて活動性の高い年齢層に多く，手関節背屈位を強制されたさいに発生する．受傷後早期の X 線像では骨折線がはっきりしないことが多く，腫脹，嗅ぎタバコ窩や舟状骨結節部の圧痛がある場合は 1～2 週間の外固定を行ったのち，再度 X 線像にて骨折の有無の確認を行う．通常の正面像，側面像では診断がむずかしく，舟状骨の長径がもっとも長く撮影されるように手を握って手関節尺屈位での正面像が有用である．舟状骨は主に遠位から骨内に侵入する橈骨動脈の枝によりほとんど栄養されているため，血行に乏しく骨癒合が得にくく偽関節となりやすい．

転位がない場合はギプスによる保存的治療が選択される．ギプス固定の範囲については議論のあるところではあるが，一般には肘下で母指は MP 関節まで含めて固定する thumb spica cast がもっとも多く用いられている．固定期間は 6～8 週間であり，その後手関節の ROM 訓練を開始する．骨癒合が得られれば通常ほぼ正常な ROM 獲得が可能である．

3 月状骨（周囲）脱臼

高所からの転落などで手関節が背屈強制され，さらに手根骨に回外強制が加わり受傷する．手関節部骨折の中ではもっとも高エネルギーによる外傷である．月状骨周囲の靱帯がすべて損傷されると，月状骨の背側にほかの手根骨が脱臼し月状骨周囲脱臼の形となる．あるいは月状骨掌側部の靱帯脆弱部であるPoirie腔より月状骨が掌側に脱臼し月状骨掌側脱臼の形となるが，両者はほぼ同じ病態と考えられている．舟状骨骨折を合併する経舟状骨月状骨周囲脱臼がもっとも多い．手関節の疼痛と腫脹が主である．著明な腫脹のため外見上は脱臼による変形が目立たないことが多い．新鮮例ではなるべく早期に整復を試みる．整復後に手根骨の配列を確認する．舟状骨月状骨間の離開，舟状骨の掌屈変形，月状骨の背屈変形が残存する場合が多く，筆者らは積極的に背側より舟状骨月状骨間靱帯の修復を行い，手根骨配列は鋼線固定にて保持する．腫脹が強いため手指のROM訓練，自動でのグリップ訓練は積極的に行ってもらう．6～8週間の外固定ののちROM訓練を開始する．前述したように投げ矢面での掌背屈は舟状骨月状骨間の動きが少なく，最初は主にこの面でのROM訓練が安全である．その後徐々に全可動方向での訓練を行う．高エネルギー外傷であり，ROM制限が残りやすいことに留意する．

4 TFCC損傷

TFCC損傷は転倒などにより手関節が背屈位，回内位で軸圧が加わったさいや繰り返す回内外ストレスにより発生する．TFCCの外傷性断裂は断裂部位により分類されている[5]．治療法として2～3ヵ月の保存的治療抵抗例では手術的治療が適応となり，手関節鏡の進歩により鏡視下手術が一般的に行われるようになった[6]．保存的治療としては，安静のため手関節中間位にてギプスシーネ固定を2～3週間施行する．シーネ除去後は取りはずし可能なスプリント固定やTFCC用のブレースを装着させる．物理療法として温熱治療を行い，回内外および掌背屈の自動運動を開始する．痛みなく自動運動が可能となった段階で他動運動，ストレッチングおよび筋力訓練を指導する．スポーツはその種類にもよるが，3ヵ月後より徐々に許可する．手術的治療として部分切除を行った場合は，1～2週間の肘下から手関節の外固定を行う．縫合術を行った場合は2週間の肘上までの固定後，さらに肘下での固定を2週間行う．外固定除去後のリハビリテーションは保存的治療と同様であるが，縫合術では腫脹が長期に及ぶため，ROM訓練は痛みの状態を観察しながら施行する．

おわりに

手関節周囲外傷後のリハビリテーションについて述べた．手関節は骨・靱帯が解剖学的に複雑な構造を呈し，そのバイオメカニクスについての知識とおのおのの手関節外傷のメカニズム，特徴についての理解も必要である．また手関節外傷後のリハビリテーションにあたっては，上肢とくに手指の機能の維持を常に考慮することが重要であると考える．

文　献

1) Ishikawa J, Cooney WP, Niebur G et al：The effects of wrist distraction on carpal kinematics. J Hand Surg **24-A**：113-120, 1999
2) Moritomo H, Murase T, Goto A et al：Capitate-based kinematics of the midcarpal joint during wrist radioulnar deviation；an *in vivo* three dimentional motion analysis. J Hand Surg **29-A**：668-675, 2004
3) 三浪明男，石川淳一：手の術後全般に関する運動療法．整形外科運動療法実践マニュアル，白土　修，宗田　大（編），全日本病院出版会，東京，p49-54，2002
4) 石川淳一，三浪明男：高齢者における橈骨遠位端骨折の治療成績．日手会誌 **18**：556-558，2002
5) Palmer AK：Triangular fibrocartilage complex lesions；a classification. J Hand Surg **14-A**：594-606, 1989
6) 石川淳一，三浪明男：TFCC損傷に対する鏡視下手術の成績．日手会誌 **19**：208-211，2002

Influence of Distal Radioulnar Joint Subluxation on Restricted Forearm Rotation After Distal Radius Fracture

Jun-ichi Ishikawa, MD, PhD, Norimasa Iwasaki, MD, PhD, Akio Minami, MD, PhD, *Sapporo, Japan*

Purpose: To analyze the influence of subluxation of the distal radioulnar joint (DRUJ) on restricted forearm rotation after distal radius fracture.

Methods: Twenty-two cases of healed unilateral distal radial fracture with restricted forearm rotation were included in the study. The subluxation of the DRUJ was evaluated using helical computed tomography scan at neutral, maximum pronation, and maximum supination and presented as the percent displacement of the ulnar head in both the injured and uninjured sides. The radiographic parameters of palmar tilt, radial inclination, dorsal shift, radial shift, and ulnar variance were measured on plain x-ray films and the rotational deformity of the distal radius was evaluated from the computed tomography scan. The differences of each radiographic parameter from the uninjured side were calculated. The relationships between the restricted forearm rotation and the percent displacement of the ulnar head and each of the radiographic parameters were analyzed statistically.

Results: When forearm pronation was restricted the ulnar head was located palmarly at neutral, maximum supination, and maximum pronation with severe dorsal tilt of the distal radius. When supination was restricted the ulnar head was located dorsally at maximum supination with severe ulnar-positive variance.

Conclusions: The subluxation of the DRUJ was related to restricted forearm rotation. The radiographic parameters of palmar tilt and ulnar variance showed an adverse influence on the position of the ulnar head at the DRUJ, which might lead to restricted forearm rotation after distal radial fracture. (J Hand Surg 2005;30A:1178–1184. Copyright © 2005 by the American Society for Surgery of the Hand.)

Type of study/level of evidence: Therapeutic, Level IV.

Key words: Distal radius fracture, forearm rotation, subluxation, distal radioulnar joint.

Restricted forearm rotation after distal radial fracture is a common problem that occurs because of subluxation of the distal radioulnar joint (DRUJ) and contracture of the surrounding soft tissues including the capsule of the DRUJ, triangular fibrocartilage, and interosseous membrane.[1] It recently was stressed that the congruity and stability of the DRUJ could be achieved when performing corrective osteotomy for malunion of the distal radius.[2–6]

Evaluation of the subluxation of the DRUJ is difficult to achieve by plain x-rays because subtle forearm rotation can lead to misinterpretation of the ulnar

From the Department of Orthopedic Surgery, Hokkaido University School of Medicine, Sapporo, Japan.

Received for publication March 2, 2005; accepted in revised form July 7, 2005.

No benefits in any form have been received or will be received from a commercial party related directly or indirectly to the subject of this article.

Corresponding author: Jun-ichi Ishikawa, MD, PhD, Department of Orthopedic Surgery, Hokkaido University School of Medicine, Kita-15, Nishi-7, Kita-ku, Sapporo 060-8638, Japan; e-mail: ishi-j@med.hokudai.ac.jp

0363-5023/05/30A06-0012$30.00/0
doi:10.1016/j.jhsa.2005.07.008

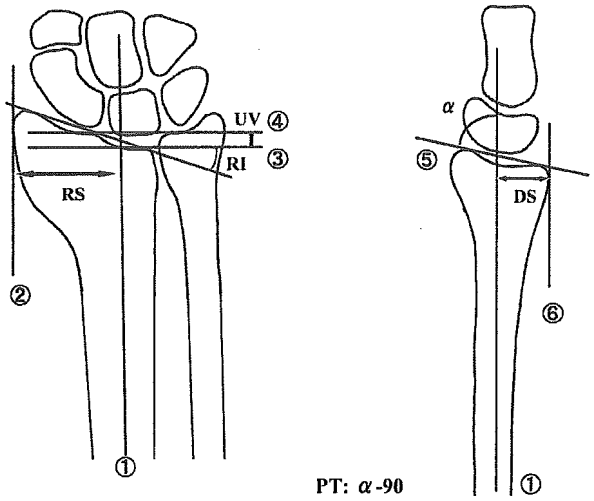

Figure 1. Each radiographic parameter was calculated as the difference between the injured and uninjured sides. (1) Longitudinal axis of the radius. (2) Line tangential to the most radial edge of the distal radius parallel to the longitudinal axis of the radius. (3) Line perpendicular to the longitudinal axis of the radius at the level of the ulnar margin of the distal radial articular surface. (4) Line perpendicular to the longitudinal axis of the distal radius at the level of the distal ulnar articular surface. (5) Line connecting the dorsal and palmar margins of the distal radial articular surface. (6) Line tangential to the most dorsal edge of the distal radius parallel to the longitudinal axis of the radius. PT, palmar tilt; RI, radial inclination; RS, radial shift; DS, dorsal shift; UV, ulnar variance.

head position. Computed tomography (CT) is a reliable radiographic tool and several investigators have advocated different methods for evaluating the subluxation with a CT scan.[7–12] There have been no reproducible methods, however, to date. Recently Lo et al[13] reported a new quantifying method to detect the subluxation of the DRUJ in a CT scan, which they termed the *radioulnar ratio*. They compared this method with other evaluation techniques (epicenter method, congruency method, and Mino criteria[10,11]) and proved the validity of their method. We have used a similar method for evaluation with a CT scan and presented it as percent displacement of the ulnar head relative to the sigmoid notch of the radius.

This *in vivo* study was designed to observe the relationship between restricted forearm rotation and subluxation of the DRUJ at neutral rotation, maximum supination, and maximum pronation and the radiographic parameters after healed distal radial fracture.

Materials and Methods

Twenty-two consecutive cases of healed unilateral distal radial fracture with restricted forearm rotation (pronation or supination) were included in the study. The initial fractures were extra-articular dorsally angulated fractures. Fractures that extended into the DRUJ and radiocarpal joint were excluded. Cases that showed restriction of both pronation and supination also were excluded to detect the influence of DRUJ subluxation on limited pronation or supination separately. The average time after the injury was 16 months (range, 6–36 mo). There were 20 women and 2 men with a mean age of 68 years (range, 29–84 y). The initial treatments for the fracture consisted of manual reduction with splint fixation (13 patients), intrafocal percutaneous pin fixation (8 patients), and external fixation (1 patient).

Palmar tilt, radial inclination, dorsal shift, radial shift of the distal radius, and ulnar variance were measured on plain posteroanterior and lateral x-rays after the fracture was healed and the differences from the uninjured side were calculated. Dorsal shift was defined as the distance between the line of the longitudinal axis of the radius and the line tangential to the most dorsal edge of the distal radius on lateral x-ray. Radial shift was defined as the distance be-

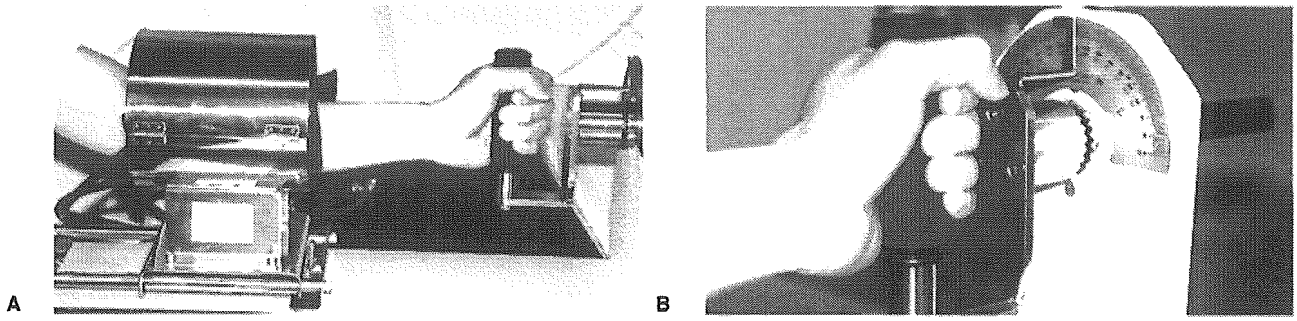

Figure 2. (A) Each patient's forearm was fixed to a custom-designed apparatus using a tourniquet band with 60° of elbow flexion. (B) The handle that gears with the protractor was locked to keep the position of forearm rotation (neutral rotation, maximum pronation, and maximum supination).

tween the line of the longitudinal axis of the radius and the line tangential to the most radial edge of the distal radius on posteroanterior x-ray (Fig. 1).[14] The ranges of each parameter were as follows: palmar tilt, −43° to 5° (average, −14°); radial inclination, −19° to 5° (average, −4°); dorsal shift, −3 to +7 mm (average, +2 mm); radial shift, −2 to +9 mm (average, +2 mm); and ulnar variance, +1 to +6 mm (average, +3 mm). In 3 cases the palmar tilt was greater than in the uninjured side because of excessive reduction of the dorsally tilted distal radial fragment during the initial treatment for the fracture.

Subluxation of the DRUJ was evaluated using helical CT scan (Xvision, Toshiba, Japan). The patients were in the prone position and the forearm was fixed to a custom-made apparatus using a tourniquet band to exclude the influence of shoulder rotation with 60° of elbow flexion (Fig. 2A). Patients were instructed to grasp the pole of the apparatus for exact positioning of the forearm rotation (Fig. 2B). To exclude rotation at the radiocarpal joint patients performed the active forearm rotation without passive forceful rotation. The degree of restricted rotation was examined using a goniometer attached to the apparatus and was confirmed on the CT scan by comparing the position of the groove for the extensor carpi ulnaris tendon in the ulnar head relative to the radius between the injured and uninjured sides.

The scan was begun from the middle of the forearm through the DRUJ at intervals of 3 mm with the forearm at neutral rotation, maximum pronation, and maximum supination. A helical CT scan of the uninjured side also was performed with the same rotational positions. Subluxation of the DRUJ at neutral rotation, maximum supination, and maximum pronation was evaluated according to the radioulnar ratio proposed by Lo et al.[13] The forearm rotational axis is a line connecting the fovea of the ulnar head distally and the center of the radial head proximally. The distal radius rotates around the ulnar head at the DRUJ. In a clinical situation, however, subluxation or dislocation at the DRUJ usually would be expressed by the position of the ulnar head. Therefore subluxation of the DRUJ was evaluated by the percent displacement of the ulnar head relative to the radius.

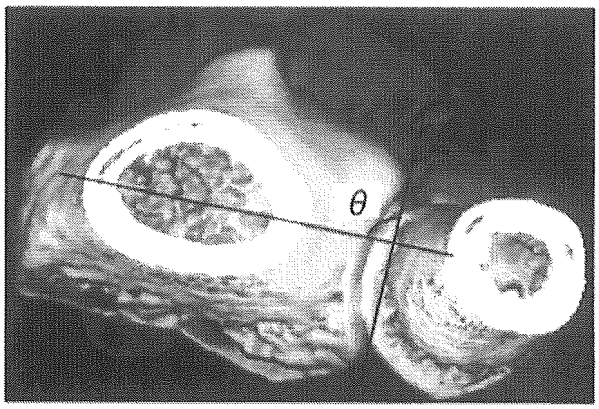

Figure 4. Pronation–supination deformity of the distal radius was determined by measuring the angle (θ) between the transverse axis of the radial shaft proximal to the site of malunion and a line tangential to the sigmoid notch of the radius from the helical CT scans at neutral rotation. The difference of the angle from the uninjured side was determined as the pronation–supination deformity. Positive = supination; negative = pronation.

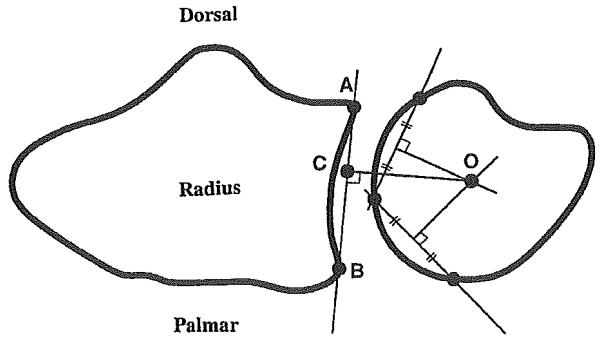

Figure 3. Percent displacement. The center of the ulnar head (O) was determined by selecting 3 points on an outline of the ulnar head. A perpendicular line was drawn to the line connecting the dorsal and palmar ridges of the sigmoid notch of the radius. The length of the palmar segment of the line (BC) was divided by the total length (AB) and presented as the percent displacement of the ulnar head. BC/AB × 100 (%) - 50 (%) was used to express the position of ulnar head; positive = palmar; negative = dorsal.

We chose the slice of the CT scan in which the ulnar head and the sigmoid notch of the radius had the largest outline of subchondral shape. If different slices were chosen for each bone then they were superimposed on each other and a 2-dimensional evaluation was performed. The center of the ulnar head was determined by selecting 3 points on an outline of the ulnar head. A line was drawn perpendicular to the line connecting the dorsal and palmar ridge of the sigmoid notch of the radius. The length of the palmar segment of the line was divided by the total length and presented as the percent displacement of the ulnar head relative to the radius (Fig. 3). The measurement was repeated 3 times and averaged at each rotational position.

The pronation–supination deformity of the distal

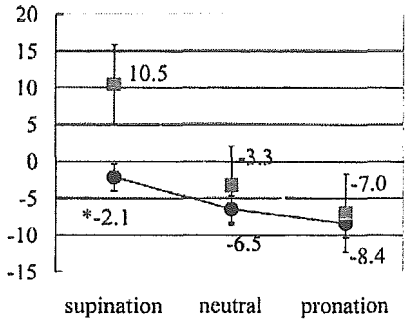

Figure 5. The percent displacement of the ulnar head in group S (restricted supination). The ulnar head on the injured side was located dorsally at supination compared with the uninjured side. *p < .05, paired *t* test between the injured and the uninjured sides. ●, Injured; ■, uninjured.

radius was added as a radiographic parameter, which was obtained by measuring the angle between a transverse axis of the radial shaft proximal to the fracture site and a line tangential to the sigmoid notch of the radius in a 3-dimensional reconstruction of the helical CT scan at neutral rotation according to the method reported by Prommersberger et al[15] (Fig. 4). The difference of the angle from the uninjured side was determined as the pronation–supination deformity (range, −15° to +11°; average, −6°; supination: +, pronation: −).

The patients were divided into 2 groups according to the direction of the limited forearm rotation: pronation or supination. The pronation was restricted (average, 24°; range, 15°–40°) in 11 patients (group P). The supination was restricted (average, 31°; range, 20°–50°) in 11 patients (group S). The percent displacement at each rotational position was compared between the injured and uninjured sides in both groups and analyzed statistically using the paired *t* test. The differences of radiographic parameters between groups P and S also were analyzed using the Student *t* test. The results of these analyses were considered significant when p values were less than .05.

Results

Percent Displacement at Each Rotational Position

The percent displacement of the ulnar head at each rotational position was compared between the injured and uninjured sides.

Restricted supination (group S). On the injured side the average percent displacements of 11 patients in group S at neutral, supination, and pronation were 7% dorsal, 2% dorsal, and 8% dorsal, respectively (Fig. 5). When compared with the uninjured side (3% dorsal, 11% palmar, 7% dorsal, respectively) the ulnar head was located dorsally at maximum supination in the injured side ($p = .034$), which means that the dorsal translation of the distal radius during forearm neutral to supination was restricted (Fig. 6).

Restricted pronation (group P). In the injured side the average percent displacements of 11 patients in group P at neutral, supination, and pronation were 17% palmar, 17% palmar, and 8% palmar, respectively (Fig. 7). When compared with the uninjured side (0% dorsal, 6% palmar, 4% dorsal, respectively) the ulnar head was located palmarly at all rotational positions on the injured side (Fig. 8) and the difference was significant at neutral rotation ($p = .039$).

Radiographic Parameters in Each Group

Each radiographic parameter was compared between the groups (Table 1). Palmar tilt and ulnar variance

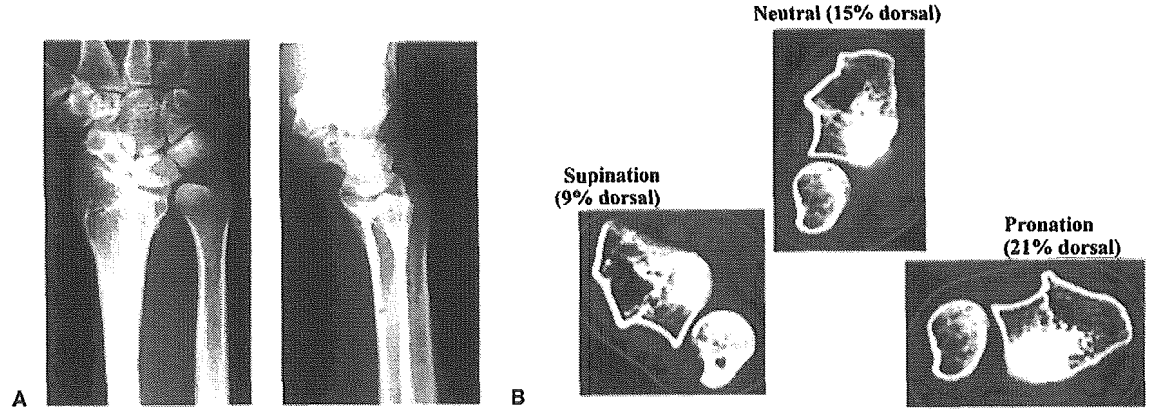

Figure 6. The injured side of the patient with restricted supination. (A) Plain x-ray shows the ulnar-positive variance (4 mm). Palmar tilt and radial inclination are nearly normal. (B) The palmar translation of the ulnar head is restricted in supination.

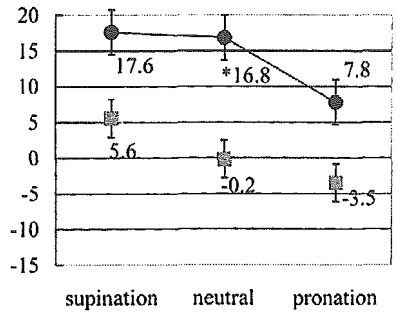

Figure 7. The percent displacement of the ulnar head in group P (restricted pronation). The ulnar head on the injured side was located palmarly at the 3 rotational positions compared with the uninjured side. *p < .05, paired *t* test between the injured and the uninjured side. ●, injured; ■, uninjured.

showed significant differences between the groups. Palmar tilt was decreased significantly greater in group P (average, −21°) than in group S (average, −6°) (p = .016). The ulnar variance was more positive in group S (average, +4 mm) than in group P (average, +2 mm) (p = .010). The other radiographic parameters showed no significant differences (radial inclination, p = .080; radial shift, p = .062; dorsal shift, p = .498; pronation–supination deformity, p = .754).

Discussion

Distal radial malunion frequently causes subluxation of the DRUJ, which can be one of the reasons for pain and limited forearm rotation on the ulnar side of the wrist.[1–6] Although several cadaveric studies have reported the effects of malunion on kinematics of the DRUJ and forearm rotation, there have been few systematic *in vivo* analyses that have shown alteration of the congruity of the DRUJ after distal radial malunion.[16–19] This study was designed to investigate the relationship between limited forearm rotation and subluxation of the DRUJ and 6 radiographic parameters including rotational deformity of the distal radius. The most reliable method to evaluate the subluxation of the DRUJ in the clinical situation would be a CT scan. The percent displacement used in this study enabled the estimation of the position of the ulnar head relative to the sigmoid notch of the radius.

Adams[16] investigated the kinematic changes by creating a deformity of the distal radius in fresh specimens and concluded that excessive radial shortening caused the greatest disturbance in kinematics of the DRUJ, whereas decreased radial inclination and dorsal angulation caused only intermediate changes. More recently Moore et al[17] investigated the 3-dimensional kinematic alterations of the DRUJ in pronation–supination after malunited distal radius fractures *in vivo* by using CT imaging. The location and orientation of the rotation axis did not change in the malunited wrists and no dorsopalmar translation at pronation–supination was detected in the study. These investigators attributed the reasons for these findings to adaptation of the soft tissues after malunited distal radius.

It has been acknowledged that the ulnar head is located palmarly relative to the distal radius in supination and dorsally in pronation because of the dorsopalmar translation of the distal radius in the normal wrist, which was recognized on the uninjured side in this study (Figs. 5, 7). On the injured side, however, the dorsopalmar position of the ulnar head at the

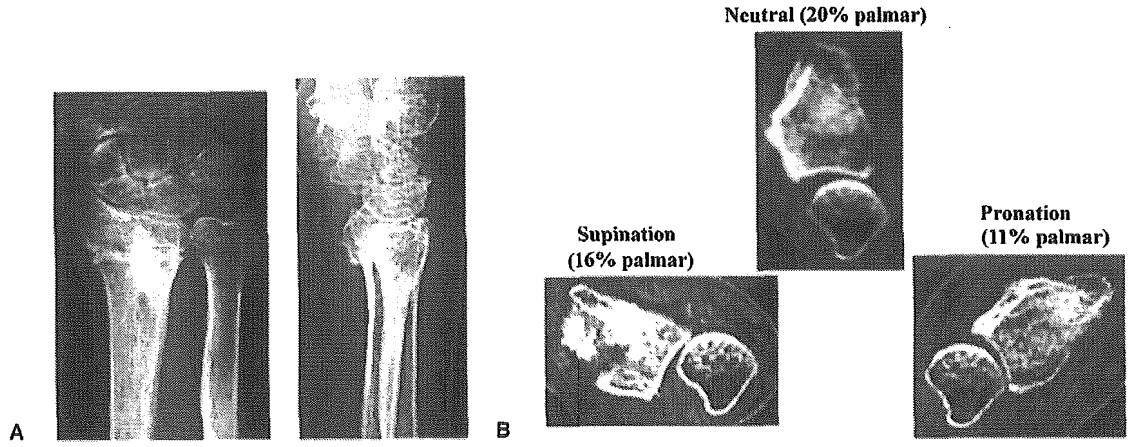

Figure 8. The injured side of the patient with restricted pronation. (A) Plain x-rays show the decreased palmar tilt (−20°). (B) The ulnar head is located palmarly at the 3 rotational positions.

Table 1. Comparison of Each Radiographic Parameter Between the Groups

	PT, degrees*	RI, degrees	UV,* mm	RS, mm	DS, mm	Pro–Supi, degrees
Restricted supination	−6.1 ± 15.2	−2.2 ± 5.4	+3.8 ± 2.0	+1.0 ± 3.1	+2.1 ± 3.0	−5.4 ± 8.7
Restricted pronation	−21.1 ± 12.4	−6.5 ± 5.4	+2.0 ± 1.3	+3.4 ± 1.5	+1.4 ± 1.7	−6.9 ± 9.2

Values are presented as the mean ± SD.
Each parameter was compared between the groups.
PT, palmar tilt; RI, radial inclination; UV, ulnar variance; RS, radial shift; DS, dorsal shift; Pro–Supi, pronation–supination deformity (+, supination; −, pronation).
*$p < .05$.

DRUJ was altered according to the deformity of the distal radius.

The position of the ulnar head showed a significant correlation with limited forearm rotation. In the group with restricted pronation the ulnar head was located palmarly at all rotational positions. By contrast in the group with restricted supination the ulnar head was located dorsally at supination. Kihara et al[18] investigated the effect of a dorsally angulated distal radius on the congruency of the DRUJ by using cadaveric specimens. In their study they concluded that the incongruency of the DRUJ occurred with a change of more than 20° of dorsal angulation of the distal radius and forearm rotation decreased significantly with dorsal angulation by more than 30°. In our study the palmar tilt of the group with restricted pronation was an average −21° compared with the uninjured side. The increased dorsal tilt caused the palmar location of the ulnar head relative to the distal radius. The malposition of the ulnar head might block the palmar translation of the radius in pronation and also elicit changes of the tension of the surrounding soft tissues including the triangular fibrocartilage complex, the capsule of the DRUJ, and the interosseous membrane, which could result in restricted pronation. By contrast the group with restricted supination showed an average ulnar-positive variance of 4 mm compared with the uninjured side. The dorsal translation of the distal radius was reduced in neutral to supination and the ulnar head was located dorsally at supination compared with the uninjured side. The severe ulnar-positive variance might block the dorsal translation of the distal radius during supination, resulting in limited supination.

With regard to the rotational deformity of the malunited distal radius Fernandez[2,3] stated that the distal fragment was flexed and pronated in Smith type fractures with dorsal subluxation of the ulnar head, which resulted in limited forearm supination. In Colles' type fractures the distal fragment was extended and supinated with palmar subluxation of the ulnar head.[2,3] The rotational deformity of the distal radius, however, showed no significant difference between the limited supination and pronation groups in our study. Prommersberger et al[15] evaluated the rotational deformity in malunited distal radius fractures and concluded that loss of pronation–supination did not correlate with the amount of rotational deformity, which is consistent with our results. In our study the number of patients was small and the rotational deformity was less than 15°, which might be why we could not detect exactly the influence of pronation–supination deformity of the distal radius on the restricted rotation. A further study will be needed to determine the effect of the rotational deformity.

From this *in vivo* study we proved the relationship between restricted forearm rotation after a healed distal radius fracture and subluxation of the DRUJ. The radiographic parameters of dorsal tilt of the distal radius and ulnar-positive variance especially showed an adverse influence on the dorsopalmar position of the ulnar head at the DRUJ, which led to limited pronation and supination.

References

1. Linscheid RL. Biomechanics of the distal radioulnar joint. Clin Orthop 1992;275:46–55.
2. Fernandez DL. Correction of post-traumatic wrist deformity in adults by osteotomy, bone-grafting, and internal fixation. J Bone Joint Surg 1982;64A:1164–1178.
3. Fernandez DL. Radial osteotomy and Bowers arthroplasty for malunited fractures of the distal end of the radius. J Bone Joint Surg 1988;70A:1538–1551.
4. Jupiter JB, Masem M. Reconstruction of post-traumatic deformity of the distal radius and ulna. Hand Clin 1988;4:377–390.
5. Jupiter JB, Ruder J, Roth DA. Computer-generated bone models in the planning of osteotomy of multidirectional distal radius malunions. J Hand Surg 1992;17A:406–415.
6. Shea K, Fernandez DL, Jupiter JB, Martin C Jr. Corrective osteotomy for malunited, volarly displaced fractures of the distal end of the radius. J Bone Joint Surg 1997;79A:1816–1826.
7. Wechsler RJ, Wehbe MA, Rifkin MD, Edeiken J, Branch

HM. Computed tomography diagnosis of distal radioulnar subluxation. Skeletal Radiol 1987;16:1–5.
8. King GJ, McMurtry RY, Rubenstein JD, Gertzbein SD. Kinematics of the distal radioulnar joint. J Hand Surg 1986; 11A:798–804.
9. King GJ, McMurtry RY, Rubenstein JD, Ogston NG. Computerized tomography of the distal radioulnar joint: correlation with ligamentous pathology in a cadaveric model. J Hand Surg 1986;11A:711–717.
10. Mino DE, Palmer AK, Levinsohn EM. Radiography and computerized tomography in the diagnosis of incongruity of the distal radio-ulnar joint. J Bone Joint Surg 1985;67A: 247–252.
11. Mino DE, Palmer AK, Levinsohn EM. The role of radiography and computerized tomography in the diagnosis of subluxation and dislocation of the distal radioulnar joint. J Hand Surg 1983;8:23–31.
12. Weiler PJ, Bogoch ER. Kinematics of the distal radioulnar joint in rheumatoid arthritis: an *in vivo* study using centrode analysis. J Hand Surg 1995;20A:937–943.
13. Lo IKY, MacDermid JC, Bennett JD, Bogoch E, King GJW. The radioulnar ratio: a new method of quantifying distal radioulnar joint subluxation. J Hand Surg 2001;26A: 236–243.
14. Kreder HJ, Hanel DP, McKee M, Jupiter J, McGillivary G, Swiontkowski MF. X-ray film measurements for healed distal radius fractures. J Hand Surg 1996;21A:31–39.
15. Prommersberger K-J, Froehner SC, Schmitt RR, Lanz UB. Rotational deformity in malunited fractures of the distal radius. J Hand Surg 2004;29A:110–115.
16. Adams BD. Effects of radial deformity on distal radioulnar joint mechanics. J Hand Surg 1993;18A:492–498.
17. Moore DC, Hogan KA, Crisco JJ III, Akelman E, DaSilva MF, Weiss A-PC. Three-dimensional *in vivo* kinematics of the distal radioulnar joint in malunited distal radius fractures. J Hand Surg 2002;27A:233–242.
18. Kihara H, Palmer AK, Werner FW, Short WH, Fortino MD. The effect of dorsally angulated distal radius fractures on distal radioulnar joint congruency and forearm rotation. J Hand Surg 1996;21A:40–47.
19. Bronstein AJ, Trumble TE, Tencer AF. The effect of distal radius fracture malalignment on forearm rotation: a cadaveric study. J Hand Surg 1997;22A:258–262.

腱板断裂時における肩甲上腕関節面の三次元応力分布

但野　茂[※1]　阿部　圭子[※1]　大泉　尚美[※2]

Stress Distribution on Glenohumeral Joint after Rotator Cuff Tears.

Shigeru TADANO, Keiko ABE, Naomi OIZUMI

Abstract

The human shoulder consists of five joints acting cooperatively to realize three dimensional mobility and stability. The shoulder joints are surrounded by the rotator cuff, which moves and slides between the humeral head and acromion during joint motion. When rotator cuff tear occurs, stress distribution on the joint surface in the glenoid is considered to change and concentrate in a local region. This diseased stress situation promotes wear of the cartilage and causes osteoarthritis of the shoulder. In this study, we made three dimensional finite element models of the glenohumeral joint. Stress distribution on the joint surface in the glenoid was analyzed for normal joints, supraspinatus tendon (SSP) tear, both supraspinatus and infraspinatus tendon (SSP-ISP) tear, and teres minor (t.minor) transfer model, at abduction angles of 45 and 90 degrees. Muscle forces calculated by numerical analysis were used as loading conditions. As a result, in an SSP tear model, the stress distribution was almost the same as in the normal model. In the SSP-ISP tear model, the stress was concentrated in the upper side in the joint surface. In the t.minor transfer model, it was confirmed that dispersion of stress occurred at a shoulder abduction angle of 45 degrees.

Key words : Biomechanics, Medical Engineering, Finite Element Method, Shoulder, Rotator cuff.

※1　北海道大学大学院　工学研究科
〒060-8628　北海道札幌市北区北13条西８丁目
※2　北海道大学大学院　医学研究科
〒060-8638　北海道札幌市北区北15条西７丁目

Corresponding Author : Shigeru TADANO
Division of Mechanical Science, Hokkaido University
Kita 13, Nishi 8, Kita-ku, Sapporo 060-8628, Japan

Tel & Fax : 011-706-6405
E-mail address : tadano@eng.hokudai.ac.jp

はじめに

肩関節は，3つの骨（上腕骨，肩甲骨，鎖骨）と胸郭が，肩甲上腕関節，肩鎖関節，胸鎖関節の解剖学的関節に加えて，肩峰下関節，肩甲胸郭関節の機能的関節も構成する．これらの関節が複雑に連動することで，大きな三次元的可動性と安定性を実現している．棘上筋腱，棘下筋腱，肩甲下筋腱，小円筋腱の合体腱である腱板は上腕骨頭周辺を取り囲み，肩関節の可動に伴い上腕骨頭と肩峰の間を滑るように動く．加齢に伴い骨棘形成などの理由で烏口肩峰アーチが狭小化すると，腱板は肩峰あるいは烏口肩峰靭帯下面との接触により徐々に摩耗し，外傷や腱自体の変性も加わって断裂することもある．肩関節は骨性支持要素が少なく腱板や靭帯などの軟組織による支持が支配的なため，腱板断裂が生じた場合，骨頭の求心性が低下して上腕骨頭の偏位など肩甲上腕関節の動態が変化し，それに伴い関節面における応力も変化すると考えられる．病的な応力の偏差は関節軟骨の摩耗を増長し，変形性肩関節症の原因となり得る．

また，広範囲腱板断裂に対する治療の1つに筋腱移行術があるが，筋腱移行による関節面の応力分布への影響を推測することは，術後の変形性肩関節症発生の機序を考える上においても重要となる．そこで本研究では三次元有限要素法により，外転運動時の正常肩甲上腕関節における表面応力の解析を行い，さらに腱板断裂肩とその治療法の1つである筋腱移行術後の応力分布も解析した．

有限要素モデルの作成

肩甲骨関節窩と上腕骨頭からなる肩甲上腕関節の三次元有限要素モデルを作成するため，まず健常ボランティア（23歳，男性）の肩関節X線CT画像を撮影した．この画像から医療用三次元画像解析ソフトAnalyze（Biomedical Imaging Resource, Rochester, MN）で骨格形状モデルを作り[6]，肩関節外形状の寸法を決定した．その値から節点座標を決め，図1の上腕骨・肩甲骨からなる有限要素モデルを作成した．モデルは3次元8節点構造要素を用いて，軟骨（Cartilage），軟骨下骨（Subchondral bone），皮質骨（Cortical bone），海綿骨（Cancellous bone）の4つの領域に分類した．また，外転角の影響を調べるため，上腕骨・肩甲骨を軟骨要素で連結したモデルを肩甲上腕関節外転45°と90°でそれぞれ作成した．節点数，要素数は45°モデルで8286，7612，90°モデルで8383，7728である．

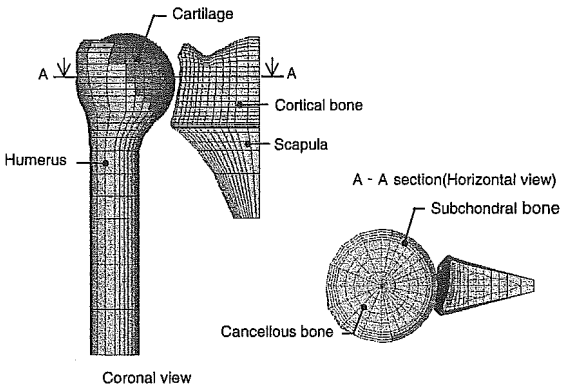

図1．Three-dimensional finite element model of glenohumeral joint with humerus and scapula.

解析方法

材料定数は文献[7]を参照し，ヤング率とポアソン比を軟骨が3 MPa/0.45，軟骨下骨が3000 MPa/0.25，皮質骨が8000MPa/0.35，海綿骨が400MPa/0.21と定義した．拘束条件は肩甲骨内側端を完全固定とした．荷重条件には，三角筋前部線維（Deltoid ant.），三角筋中部線維（Deltoid mid.），三角筋後部線維（Deltoid

post.)，棘上筋（Supraspinatus)，棘下筋（Infraspinatus)，肩甲下筋（Subscapularis)，小円筋（Teres minor）の計７筋の筋力を用いた．各筋力は筋の停止点に作用するものとし，著者らの過去の報告[6]から筋の停止座標，作用ベクトルを引用し，数値解析を行って計算により筋力を求めた．一例として，外転45°の正常モデルにおける解析条件を図２に示す．荷重条件の異なる解析として，(1)正常モデル，(2)棘上筋腱（SSP）断裂モデル，(3)棘上筋・棘下筋腱（SSP-ISP）断裂モデル，(4)腱板断裂に対する筋腱移行術の１つである小円筋腱移行モデル，の計４種類を設定した．SSP断裂モデルおよびSSP-ISP断裂モデルでは，各筋腱の完全断裂を想定し，断裂筋を除いた数値解析を行って筋力を求めた．小円筋腱移行モデルでは，小円筋の停止位置を棘上筋の停止位置に移行して数値解析を行った．計算によって得られた外転45°と90°における筋力値を表１に示す．

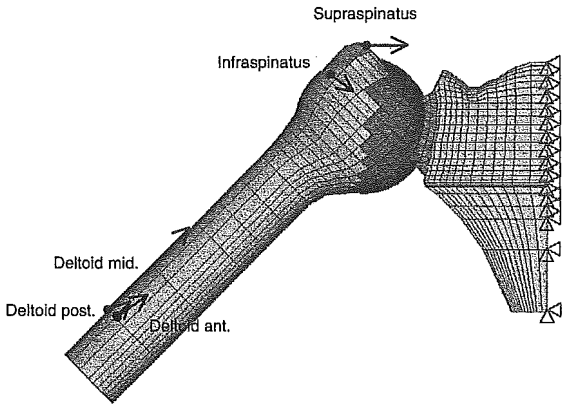

図２．Loading condition of normal model in abduction angle 45 degrees.

表１．a：Muscle force in abduction angle 45 degrees.
b：Muscle force in abduction angle 90 degrees.

(a)

Muscle	Normal	SSP tear	SSP-ISP tear	T.minor transfer
Deltoid ant.	61	76	84	28
Deltoid mid.	207	266	314	272
Deltoid post.	19	35	56	0
Supraspinatus	70	0	0	0
Infraspinatus	62	51	0	0
Subscapularis	0	0	0	0
Teres minor	0	0	41	97

(N)

(b)

Muscle	Normal	SSP tear	SSP-ISP tear	T.minor transfer
Deltoid ant.	87	101	121	134
Deltoid mid.	257	297	342	332
Deltoid post.	63	71	113	64
Supraspinatus	80	0	0	0
Infraspinatus	68	80	0	0
Subscapularis	50	62	75	105
Teres minor	19	23	67	75

(N)

共同著者の大泉ら[5]はMRIを用いて正常肩と腱板断裂肩の外転運動時の動態解析を行い，棘上筋腱単独の断裂では上腕骨頭は関節窩に対して求心位を保つが，棘上筋・棘下筋腱断裂の場合には，上腕骨頭が上方へ移動することを報告している．その結果を踏まえ，SSP-ISP断裂モデルと小円筋腱移行モデルでは上腕骨頭中心を４mm上方に移動させた．解析には有限要素解析ソフトANSYS5. 5. 2（ANSYS Inc, USA）を使用し，静解析を行った．

解析結果は，肩甲骨関節窩軟骨要素に生じる圧縮応力分布と最大圧縮応力値を各モデルにおいて比較評価した．さらに，応力の集中範囲を定量化するために，関節窩軟骨要素に生じた全圧縮応力領域に対する応力集中領域の割合（Stress Concentration Area/Total Compression Stress Area，以下SCA/TCSA）を求めた．ここでSCAは，正常モデルの最大圧縮応力の80%以上の応力になる面積と定義した．ANSYSでの解析結果を画像解析ソフトScion Image for Windows Bata 4. 0. 2（Scion Corporation, USA）に取り込んで，SCA，TCSAそれぞれの面積を測定した．SCA/TCSAの値が大きいほど関節窩における高応力領域が大きいことを表している．

結　　果

１．関節面に生じる圧縮応力分布

外転45°および90°での関節面に生じる圧縮応力の分布を図３，図４に示す．全てのモデルにおいて関節面上方部に圧縮応力が生じており，外転45°に比べ外転90°では応力値が高くなり，応力発生領域が広くなっていた．正常モデ

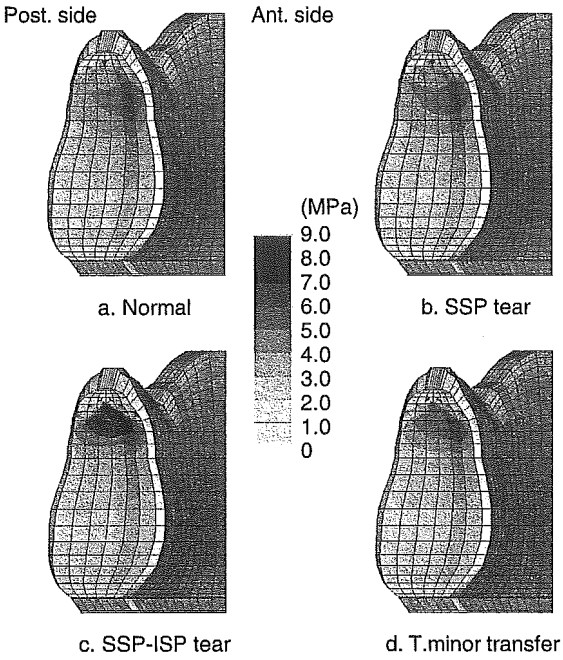

図3. Compression stress distribution in cartilage element of glenoid in abduction angle 45 degrees. (a : Normal model, b : SSP tear model, c : SSP-ISP tear model, d : T.minor transfer model.)

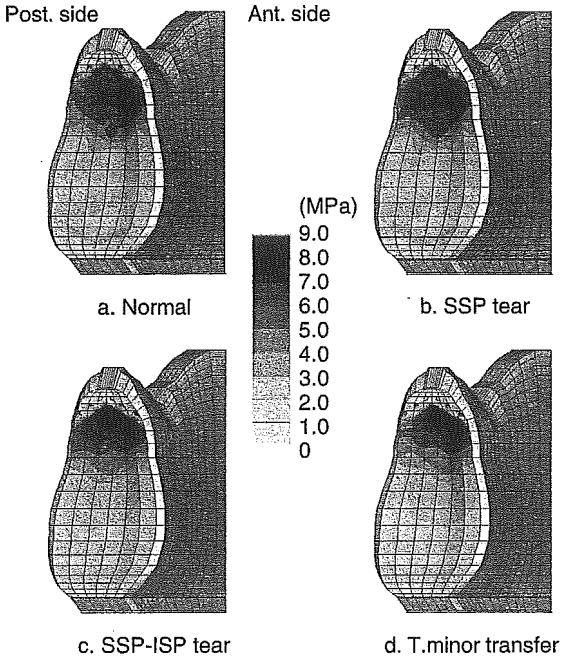

図4. Compression stress distribution in cartilage element of glenoid in abduction angle 90 degrees. (a : Normal model, b : SSP tear model, c : SSP-ISP tear model, d : T.minor transfer model.)

ルと比較してSSP断裂モデルでは外転45°, 90°ともにその応力分布に大きな変化は見られなかった. しかし, SSP-ISP断裂モデルでは応力値は増加し, より上方へ移動していた. 小円筋腱移行モデルをSSP-ISPモデルと比較すると, 外転45°では応力値が減少しているが, 外転90°では応力の変化は見られなかった.

2. 最大圧縮応力値

外転45°および90°における最大圧縮応力値を図5に示す. どのモデルにおいても外転45°よりも外転90°で大きな値となった. 外転45°では正常, SSP断裂モデルの間に差はなく, SSP-ISP断裂モデルが一番大きな値となり, 続いて小円筋腱移行モデルが大きな値を示した. 外転90°においては, 正常とSSP断裂モデル, SSP-ISP断裂と小円筋腱移行モデルの間に大きな差は見られなかった. 後者は前者より大きな値を示した.

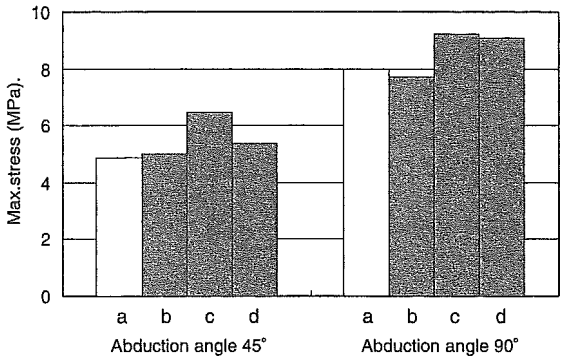

図5. Maximum compression stress in abduction angle 45 and 90 degrees. (a : Normal model, b : SSP tear model, c : SSP-ISP tear model, d : T.minor transfer model.)

3. 応力集中領域の割合

外転45°および90°におけるSCA/TCSAの値を図6に示す. 外転45°では, 正常モデルとSSP断裂モデルの間でそれほど変化はないが, SSP-ISP断裂モデルの値は正常モデルの約2倍となっていた. 小円筋腱移行モデルではSCA/TCSAの値は大幅に減少し, 正常モデルの値に近づいていた. 外転90°の場合には正常, SSP断裂モデルの間で大きな変化はなかったが, SSP-ISP断裂モデルでは正常の2倍以上の値とな

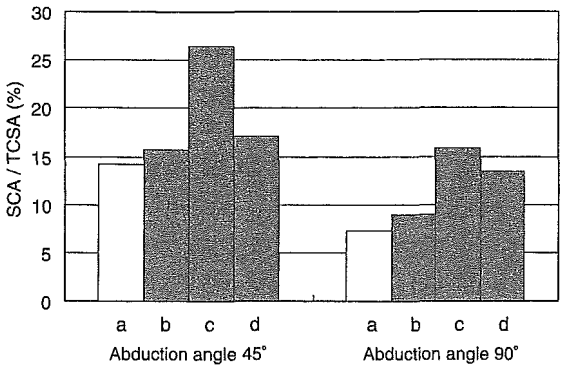

図6. SCA/TCSA value in abduction angle 45 and 90 degrees. (a : Normal model, b : SSP tear model, c : SSP-ISP tear model, d : T.minor transfer model.)

り，小円筋腱移行モデルでは若干減少するものの依然として高い値を示した．

考　　察

複雑な形状を有する生体構造の有限要素解析は，近年のコンピュータ技術の発展によって急速に進歩した．肩関節については人工関節の形状検討を目的とする解析[1)~4),7)]が多く，正常肩関節，および腱板断裂肩の解析はほとんど行われていない．本研究では，CT画像をもとに肩関節の三次元有限要素モデルを作成し，正常肩関節，腱板断裂肩と筋腱移行術後の解析を行った．その結果，正常モデルとSSP断裂モデルでは応力分布に大きな変化は見られなかったが，SSP-ISP断裂モデルの場合には応力値の増加と高応力領域の増大が確認できた．また，外転45°においては，SSP-ISP断裂モデルに比べて小円筋腱移行モデルでは最大応力値とSCA/TCSAの値が正常モデルの値に近づいており，これはSSP-ISP断裂により生じた過度の応力集中が，腱移行により改善されたことを示すと考えられた．しかし，外転90°ではSSP-ISP断裂モデルと小円筋腱移行モデルの応力状態に大きな変化はなく，腱移行による応力の分散化の効果は認められなかった．

これまで肩甲上腕関節における有限要素解析においては，関節面の複数の点，あるいは面に直接荷重を加える報告[1)~4)]が多かった．また，Stoneら[7)]は腱板断裂をシミュレーションするため，関節面にかかる荷重ベクトルを仮定しているが，腱板断裂時の荷重条件は未だ不確定である．本解析では，上腕骨も含めたモデルを作成して，直接荷重ではなく各筋力を筋の停止位置に負荷することにより，生体内における実際の荷重条件により近い状態を再現できるようにした．また，数値解析を用いて腱板断裂時，筋腱移行時の各筋力を計算し，荷重条件として導入することができた．本手法により，各種の腱断裂，筋腱移行術などのシミュレーションが可能となった．また，本解析では上腕骨・肩甲骨を連結モデルとして，異なる荷重条件による応力分布の変化をとらえることができた．しかし，今後は関節面における接触状態を考慮したモデルでの解析が必要と考えている．

ま と め

1．肩甲上腕関節の三次元有限要素モデルを作成し，筋力数値解析の結果を用いて解析を行い，外転運動時における肩甲骨関節窩軟骨要素の応力分布を検討した．
2．棘上筋腱断裂モデルでは応力分布に大きな変化は現れないが，棘上筋・棘下筋腱断裂モデルでは最大圧縮応力値の増加と高応力領域の増大が見られた．
3．棘上筋・棘下筋腱断裂モデルと比較して小円筋腱移行モデルにおいては，外転45°では腱移行による応力分散効果が認められたが，外転90°では明らかな変化は見られなかった．

文　　献

1）Couteau B, Mansat P et al. : Finite element analysis of the mechanical behavior of a scapula implanted with a glenoid prosthesis. Clinical Biomechanics, 16 : 566-575, 2001.
2）Friedman JR, Dooley LR et al. : Finite element modeling of the glenoid component : Effect of design parameters on stress distribution. Journal of Shoulder and Elbow Surgery, 1 (5) : 261-270, 1992.

3）Lacroix D, Murphy LA et al. : Three-Dimensional Finite Element Analysis of Glenoid Replacement Prostheses : A Comparison of Keeled and Pegged Anchorage Systems. Journal of Biomechanical Engineering, 122 : 430-436, 2000.
4）Murphy LA, Prendergast PJ et al. : Structural analysis of an offset-keel design glenoid component compared with a center-keel design. Journal of Shoulder and Elbow Surgery, 10 (6) : 568-579, 2001.
5）大泉尚美, 末永直樹 他：Open MRIを用いた肩関節自動外転運動時の動態解析. 日本肩関節学会誌, 26 (3)：481-485, 2002.
6）大泉尚美, 但野茂 他：三次元骨格筋モデルを用いた肩関節外転運動時の筋力数値解析. 日本機械学会論文集, 69 (677-A)：77-83, 2003.
7）Stone KD, Grabowski JJ et al. : Stress analyses of glenoid components in total shoulder arthroplasty. Journal of Shoulder and Elbow Surgery, 8 (2) : 151-158, 1999.